LETTER

doi:10.1038/nature09620

Pleats in crystals on curved surfaces

William T. M. Irvine[1]†, Vincenzo Vitelli[2] & Paul M. Chaikin[1]

Hexagons can easily tile a flat surface, but not a curved one. Introducing heptagons and pentagons (defects with topological charge) makes it easier to tile curved surfaces; for example, soccer balls based on the geodesic domes[1] of Buckminster Fuller have exactly 12 pentagons (positive charges). Interacting particles that invariably form hexagonal crystals on a plane exhibit fascinating scarred defect patterns on a sphere[2–4]. Here we show that, for more general curved surfaces, curvature may be relaxed by pleats: uncharged lines of dislocations (topological dipoles) that vanish on the surface and play the same role as fabric pleats. We experimentally investigate crystal order on surfaces with spatially varying positive and negative curvature. On cylindrical capillary bridges, stretched to produce negative curvature, we observe a sequence of transitions—consistent with our energetic calculations—from no defects to isolated dislocations, which subsequently proliferate and organize into pleats; finally, scars and isolated heptagons (previously unseen) appear. This fine control of crystal order with curvature will enable explorations of general theories of defects in curved spaces[5–11]. From a practical viewpoint, it may be possible to engineer structures with curvature (such as waisted nanotubes and vaulted architecture) and to develop novel methods for soft lithography[12] and directed self-assembly[13].

Topological defects have played a crucial role in understanding the order, rigidity and melting of crystals and other phases of matter in two-dimensional flat space[14,15]. On a curved surface (Fig. 1), these particle-like excitations acquire a new life: they interact not only with each other, but with the curvature of the substrate. In a hexagonal lattice in which every particle has six nearest neighbours (Fig. 1, inset), there are two types of topological defects (Fig. 2): disclinations that disrupt orientational order and appear as points of local five-fold or seven-fold symmetry, (pentagons or heptagons, having topological charge $\pm(2\pi/6)$, and dislocations, which disrupt translational order and appear as disclination dipoles (+/− pairs). That disclinations couple to curvature can be understood intuitively by taking a piece of paper, and adding, or removing, a $\pi/3$ wedge to 'make' a disclination, Fig. 2c, d.

A host of new discoveries[2,4,7,16] have resulted from studies of these defects on the simplest curved surface: the sphere. With increasing size, the familiar 12-pentagon soccer ball pattern gives way to 'scars', pentagons dressed by strings of dislocations[2–4]. In this Letter, we introduce a different configuration of dislocations, namely, 'pleats'—topologically uncharged grain boundaries with variable spacing that vanish on the surface. We experimentally investigate their interaction with curvature and show when pleats are energetically favoured over undefected crystals or topologically charged disclinations. Apart from experiments on spheres, and bubble bearing paraboloids[17], the interaction of defects with variable curvature, negative curvature and surfaces of different topologies has remained largely unexplored experimentally and is of growing theoretical interest[8–11,18–20].

The topology of surfaces[21] places a constraint on the total defect charge—for example the net charge on a sphere must be 4π, as exemplified by a soccer ball that has 12 ($=4\pi/(\pi/3)$) pentagons dispersed among hexagons. A hemisphere, or disk, requires half the topological

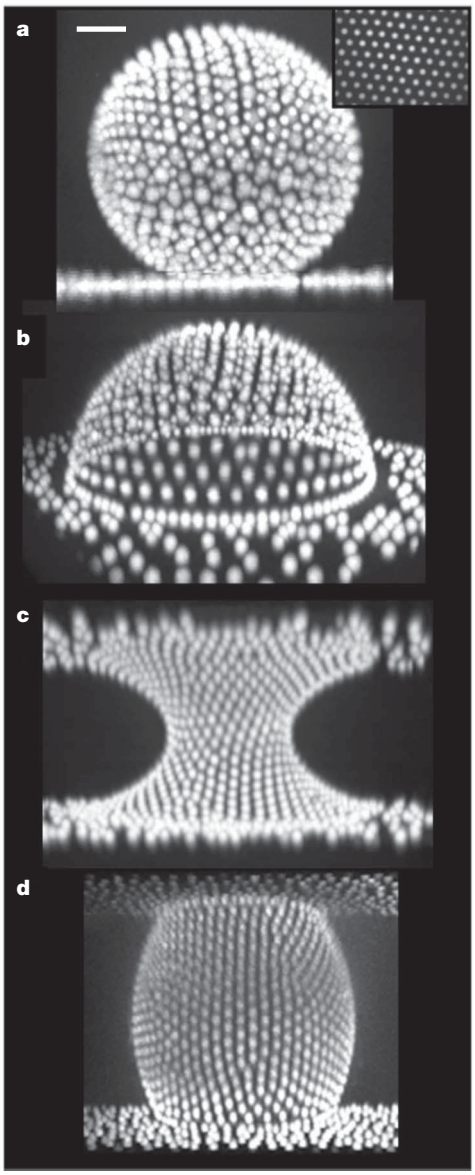

Figure 1 | Colloidal crystals on curved oil–glycerol interfaces. **a–d**, Fluorescent PMMA particles bound, by image attraction, to oil–glycerol interfaces in the shape of spheres (**a**), domes (**b**), waists (**c**) and barrels (**d**) (see Supplementary Information section 2 for details of shape). The particles interact via a repulsive screened Coulomb interaction and, on a flat surface, arrange into a hexagonal crystal lattice (**a**, inset). The oil phase is a mixture of cyclohexyl bromide and dodecane that matches the refractive index of glycerol, allowing us to image particles on highly curved interfaces by confocal microscopy. Because of their topology, crystals on spheres and domes require a net defect charge of $12\times(2\pi/6)$ and $6\times(2\pi/6)$, respectively, whereas waists and barrels require none. While spheres (**a**) have no boundary, the remaining surfaces (**b–d**) do, allowing topological defects a choice between boundary and bulk.

[1]Center for Soft Matter Research, Department of Physics, New York University, 4 Washington Place, New York, New York 10003, USA. [2]Instituut-Lorentz for Theoretical Physics, Leiden University, 271, Niels Bohrweg 2 Leiden, NL 2333 CA, The Netherlands. †Present address: James Franck Institute and Department of Physics, The University of Chicago, Chicago, Illinois 60637, USA.

charge of a sphere, whereas a cylinder can be defect-free with a requirement of 0 total charge.

Topology constrains the total charge, but it is energetics that determines the number and the arrangement of each charge. In elasticity theory[15], disclinations appear as discrete interacting charges and the Gaussian curvature as a charge density, both acting as sources of stress:

$$\frac{1}{Y}\nabla^4\chi = G(x) - \sum_\alpha q_\alpha \delta(x - x_\alpha) \quad (1)$$

where $G = \frac{1}{R_1}\frac{1}{R_2}$ is the Gaussian curvature (with R_1 and R_2 the principal radii of curvature), q_α is the charge of the disclination at x_α, δ represents a Dirac delta function, Y is Young's modulus and χ is the Airy stress function—and we will refer to the partial or complete cancellation of the effects of curvature and stress by topological charges (r.h.s. of equation (1)) as screening. For curvature concentrated at a point, as in our model paper disclinations of Fig. 2c, the screening can be perfect, the lattice is stress free and the energy $E = \frac{1}{2Y}\int \left(\nabla^2\chi\right)^2 \mathrm{d}A = 0$ (where we have assumed no bending energy). For smooth surfaces, the screening is more subtle. Geometry provides some insight: consider a geodesic triangle drawn on a curved surface, for example, a sphere. Curvature causes lines to diverge or converge, affecting the angles at the vertices: the sum of the external angles will differ from 2π by $\Delta\theta = \int G\mathrm{d}A$. The same applies to any closed loop formed by connecting lattice sites and serves as a measure of angular strain. If instead, a disclination is encircled by the loop, by definition this adds/removes a contribution of $\pm(2\pi/6)$ regardless of the size of the loop. If sufficient curvature is enclosed, the angular stress generated by the disclination is screened on the outside. Within the patch the screening is incomplete and leads to an energetic cost. For later use we define $\Omega = \frac{1}{\pi/3}\int G\,\mathrm{d}A$, the integrated curvature in units of disclinations.

The crystals we create consist of poly(methyl methacrylate) (PMMA) particles (~2 μm diameter) that are bound to an oil–glycerol interface and repel each other. By index-matching the oil to the glycerol, we can image the full surfaces (Fig. 1, Methods). The first surfaces we investigate are domes (truncated spheres), created by droplets sitting on a coverslip, with a circular contact line. The contact angle, controlled by treating the glass surface, determines the solid angle of the spherical droplet.

The domes (Fig. 3) exhibit both disclinations and scars as previously seen on spherical surfaces. However, for domes, the net disclination charge on the surface can vary as the dome inflates from a disk to a full sphere. In Fig. 3b we show the topological charge that is on the surface of the dome and detached from the boundary as a function of Ω. We find the intuitive result that the detached charge varies approximately linearly with Ω. That is, for a full sphere there are 12 pentagons ($+\pi/3$)s, for a hemisphere there are 6 pentagons ($+\pi/3$)s and on smaller fractions the two remain approximately proportional. Note that the topological requirement of a total of 6 ($+\pi/3$)s is satisfied at all times by compensating charges on the boundary.

Negative curvature surfaces lack the simplicity and familiarity that we associate with positive curvature surfaces such as the sphere. For

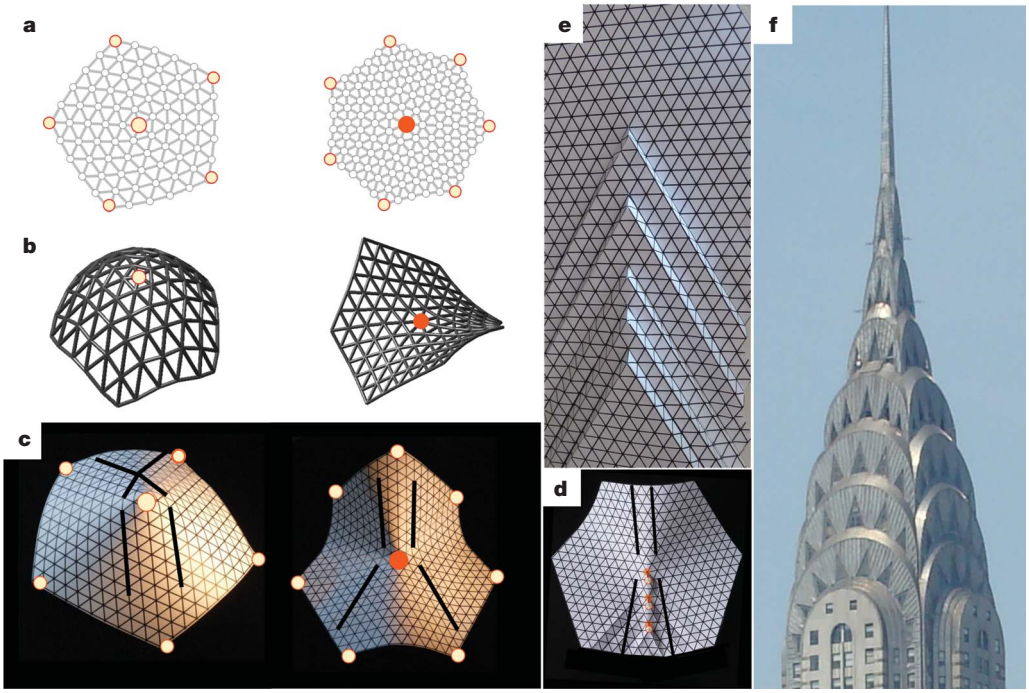

Figure 2 | Disclinations and pleats in a hexagonal lattice. **a**, Disclinations in a hexagonal lattice are topological defects that result from an extra (right panels) or missing (left panels) 60° crystalline wedge that matches their topological charge of $+/-(2\pi/6)$ marked here by cream/brick circles, respectively. At the 'core' of the disclination is a corresponding five-fold (or seven-fold) coordinated particle. In flat space, disclinations produce a large amount of stress in a crystal, disrupting orientational order. **b**, This stress can be relieved by buckling the crystal to create a curved surface. Five-fold disclinations are sources of positive Gaussian curvature, seven-fold disclinations of negative curvature. **c**, This coupling can be intuitively understood by making disclinations out of paper (see Supplementary Information for instructions and cut-outs). Paper can be bent much more easily than it can be stretched/compressed, so it bends, resulting in a surface free of stress, with all the Gaussian curvature concentrated at the locations of the disclinations. Neighbouring crystal planes diverge on these surfaces, matching the geodesics of the curved surface. **d**, Dislocations, uncharged pairs of seven- and five-fold disclinations, can also be made by folding and gluing hexagonal paper. A set of three closely spaced, aligned dislocations (7-5,7-5,7-5) are shown on an approximately relaxed sheet. This is a grain boundary which vanishes at the centre of the sheet—a 'pleat'. Note that negative curvature emanates from the vanishing point of the pleat, as evidenced both by the buckling of the sheet and by the 30° divergence of parallel lines impinging from the top. **e**, A stress-free pleat can be achieved by allowing steps out of the surface. The pleat retains the property that width is added along the pleat length in proportion to the linear density of dislocations. **f**, The top of the Chrysler building in New York consists of four vertical pleats on a cylinder. Here the pleats are formed from dislocations in a square field. Counting from the top, steps 3, 4, 5, 6 are approximately equally spaced at 8.4 m and form a cone with no Gaussian curvature. A gradient in linear dislocation density is achieved by spacing the second and first step at 9.4 m and 9.8 m spacing, resulting in a spike with negative Gaussian curvature crowning the cone.

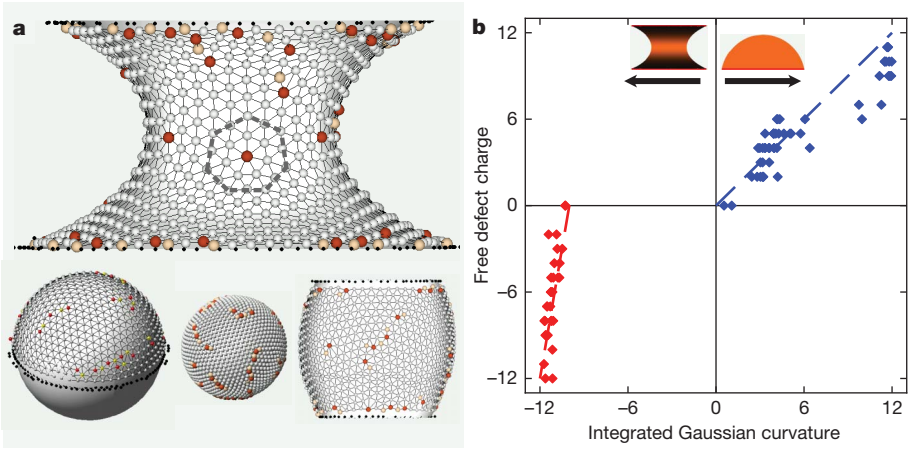

Figure 3 | Topological charge on domes and waists. **a**, Isolated seven-fold disclinations, observed here for the first time, can be seen at the neck of the capillary bridge (top). On the dome, sphere and barrel (bottom), the defects group into grain boundaries each having a single five-fold disclination in excess. The angular length of these scars is uniform, the number of dislocations depends only on R/a. The defect configurations on both surfaces are similar to the arrangement of defects on the surface of a sphere with no boundary. Both surfaces have uniform positive curvature. The black dots represent particles stuck to the glass surface, defects with charge $+\pi/3$ are coloured brick, defects with charge $-\pi/3$ are coloured cream. **b**, Detached topological charge on domes and waists versus the integrated Gaussian curvature, Ω. Detached charge is the sum of the charge of isolated disclinations and of scars that are not connected to the boundary. On domes (blue symbols), we find the intuitive result that there is approximately one ($\pi/3$) topological charge per unit's $\pi/3$ worth of integrated curvature. On negatively curved capillary bridges (red symbols), we find no net disclinations on the surface for an integrated curvature down to -10. For total curvature beyond the threshold of -10, disclinations rapidly fill the surface until 12 ($-\pi/3$) disclinations match the $\Omega = -12$ curvature. The dashed lines are guides to the eye.

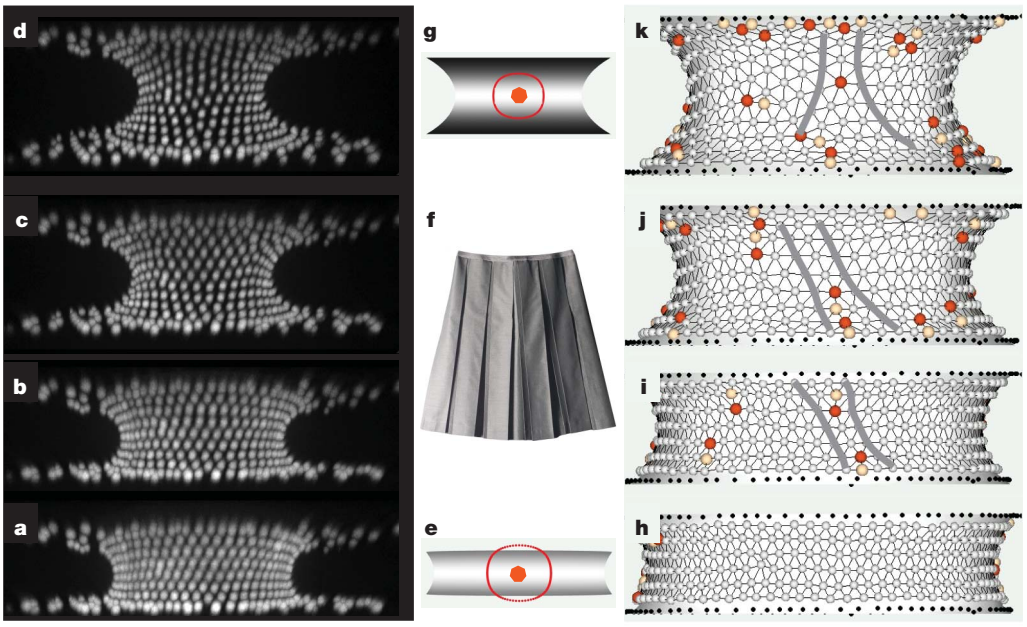

Figure 4 | Pleating and disclination unbinding on a stretched capillary bridge. **a**–**d**, Confocal images of a capillary bridge that was stretched from quasi-cylindrical to highly curved. **h**–**k**, The corresponding reconstructed and triangulated surfaces. **a**, **h**, The compressed bridge exhibits very few defects. In this regime, the bridge is weakly curved and therefore a large patch of integrated curvature is required to screen the charge of a disclination. The circle that encloses such a patch is shown in **e**; clearly its radius exceeds the height of the bridge. As the bridge is stretched (**i**–**j**), we observe the appearance of dislocations, neutral disclination dipoles, polarized with the seven-fold defects towards the maximally negatively curved neck. The crystal planes can be seen to diverge around these dislocation pairs, healing the stress induced by the negative curvature. As the bridge is stretched further, these dislocations proliferate, forming 'pleats', neutral grain boundaries that vanish in proximity of the neck. Uniform pleats on a skirt (**f**) reduce the circumference with height, producing a conical shape. Decreasing the pleat density with height would lead to negative curvature flaring the skirt. The divergence of the crystal planes at the opening of a high-density pleat (grey lines) is roughly half that observed around an isolated disclination (**k**). Finally, as the size of a patch required to screen the topological charge of an isolated seven-fold defect fits on the surface (**g**), we observe the appearance of isolated disclinations.

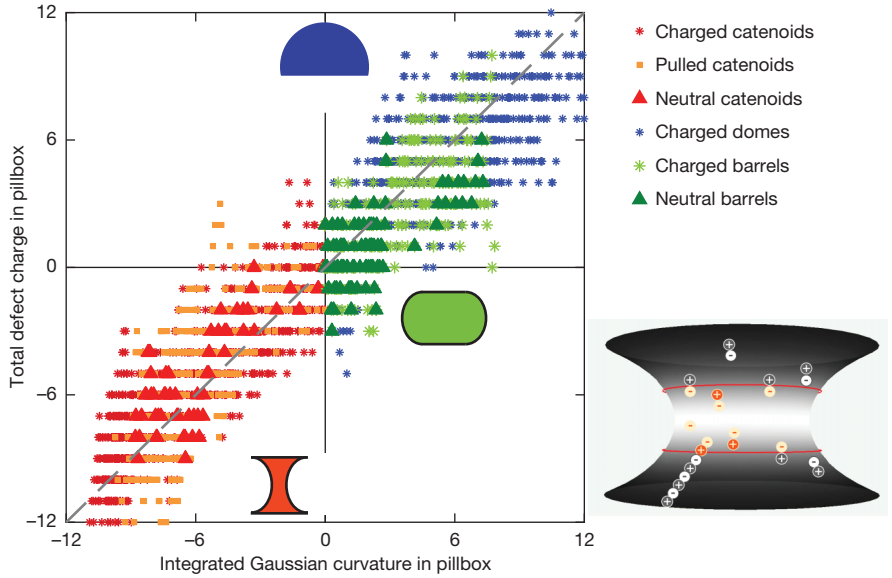

Figure 5 | Disclination and polarization charge on the surfaces of waists, domes and barrels. On each surface in our ensemble, we considered a patch ('pillbox') of variable size, for example as represented by the area between the red lines in the inset (bottom right) and computed the integrated Gaussian curvature (horizontal axis) versus the accumulated disclination plus polarization charge in the patch (vertical axis). All topological charges in the patch (excluding the edges) contribute, whether isolated or connected by a pleat to the edge. Once pleats and scars are taken into account, we regain the intuitive result of a linear relation between Gaussian curvature and defect charge. Note that the triangular symbols correspond to samples with no detached charge on the surface.

example, it is not possible to embed a complete pseudo-sphere (sphere of negative curvature) in three-dimensional space. We create negative curvature surfaces by forming capillary bridges between two surfaces treated to have partially wetting glycerol contacts. These surfaces, shown in Figs 1, 3 and 4, are constrained to have constant mean curvature, $\frac{1}{R_1}+\frac{1}{R_2}$, and enclose a fixed volume. They are unduloids, nodoids and for some specific constructions catenoids or sections of spheres[22,23] (See Supplementary Information section 2). Topologically equivalent to cylinders and therefore requiring zero net charge, these surfaces typically have varying Gaussian curvature, as shown by the colour shading in Fig. 3b. On highly curved surfaces, we observe isolated $-\pi/3$ disclinations (heptagons) for the first time (Fig. 3a). These are the negative curvature counterpart of the pentagons on the sphere and can also appear as 'scars' with an excess heptagon. However, if we plot (Fig. 3) the charge detached from the boundary versus Ω for an ensemble of capillary bridges, we find no net topological charge on the surface for an integrated curvature down to -10. For total curvature beyond this threshold, disclinations rapidly fill the surface until 12 heptagons, each $(-\pi/3)$, match the $\Omega=-12$ curvature. If no isolated charges are present below threshold, how does the crystal screen the curvature? A glance at surfaces below threshold (Fig. 4i, j) immediately suggests an answer: charge neutral dislocations.

To investigate this regime, we pulled apart the coverslips that confine the capillary bridges. As the boundary of the bridges is pinned and their volume conserved, their shape changes from almost cylindrical to highly curved, allowing us to follow the introduction of defects below threshold (see Fig. 4). The first defects that we observe as the (negative) curvature is increased are dislocations, dominantly polarized with their $(-\pi/3)$ disclinations pointing towards the region of highest negative curvature, the waist of the capillary bridge. As the integrated negative curvature is increased, these polarized dislocations proliferate and organize into lines. In flat space these lines, known as grain boundaries, close on themselves or span the whole sample. Here we observe neutral grain boundaries which vanish on the surface. They are analogous to fabric 'pleats'. In clothing, the different circumference of the waist and the hips is often accommodated by vertical pleats (Fig. 4f). Along the length of the pleat, extra fabric is added to the width.

At the point where the pleat begins, the opening angle $\Delta\theta$ is determined by the dislocation line density n_d according to[24]

$$\Delta\theta = n_d 2a\frac{\pi}{6} \qquad (2)$$

where a is the lattice spacing. If $\Delta\theta$ perfectly matches the integrated Gaussian curvature, the stress induced by the substrate is completely screened. The smallest $\Delta\theta$ is achieved by a pleat for which n_d is so low that only a single dislocation is present on a surface of characteristic length H. Equation (2) then gives a geometric criterion for the onset of pleating: $\Delta\theta=\left|\int G\mathrm{d}A\right|\approx a/H$ which can be arbitrarily small. Perfect screening cannot be achieved on a smooth surface. However, balancing the energy of a stretched but un-defected crystal, $Y\Delta\theta^2H^2$, with the energy of a pleat, $YaH\Delta\theta\log(\Delta\theta)$, gives an energetic criterion for the onset of pleating, $\left|\int G\mathrm{d}A\right|\approx(a/H)\log(H/a)$, that agrees with the geometric criterion up to logarithmic corrections (Supplementary Information).

There is a maximum opening angle for pleats $\Delta\theta_{\max}=\frac{\pi}{6}$ that corresponds to the maximum dislocation line density $n_d=\frac{1}{2a}$ in equation (2), see Fig. 2d. If we place these pleats along the axis of a cylinder the result is a cone, as illustrated in Fig. 2f, which shows the conical shape of the top of the Chrysler building, in New York. If the dislocation density in the pleats (or the density of pleats) varies, then we can have Gaussian curvature. On the Chrysler building, such a gradient in spacing produces a negative curvature spike that crowns the cone.

When our capillary bridges are strongly curved, multiple pleats and scars act in concert to relieve the strain induced by the curvature. This cooperative screening can be understood by treating dislocations as dipoles of disclinations. Just as in electrostatics, a divergence in polarization produces a polarization charge, pleat gradients can produce an effective disclination polarization charge, which along with isolated disclinations contributes to screen curvature so that

$$\int G\,\mathrm{d}A \approx \sum_{\alpha=1}^{n} q_\alpha + \int \mathrm{d}A\ \nabla\cdot P(x) \qquad (3)$$

where P(x) is the dislocation density per unit area. In Fig. 5, we verify that the integrated Gaussian curvature over a 'patch' of variable size on each surface in our ensemble (including domes, barrels and waists) is approximately equal to the accumulated disclination and polarization

charges in the patch (excluding surface edges), for all regimes of deformation.

Pleats allow a finer screening of curvature than scars, as the angular deficit produced by disclinations is not tunable but quantized in units of $\pi/3$. Upon equating $\pi/3$ to the Gaussian curvature multiplied by the area of a patch of radius r, we have a heuristic criterion for scarring $r=\sqrt{\frac{R_1R_2}{3}}$ that is consistent with our observations. If the distance to the boundary of our curved substrates is greater than r, isolated disclinations or scars are observed; if less than r, pleats arise as the generic mode of stress relaxation.

In summary, pleats (neutral dislocation lines that vanish on the on the surface) afford a much finer screening of Gaussian curvature than do disclinations of quantized topological charge, because the area surrounding the vanishing point of a pleat can have a continuously controllable angle deficit between 0 and $\pi/6$. Whether pleats may have a role to play in the design of geodetic-dome-like structures with equal length struts we leave open for exploration. Beyond the physics of crystalline defects, the experimental playground we have developed is ideal for exploring general questions concerning the physics of order and disorder[25] in curved space.

METHODS SUMMARY

Sample preparation. The oil–glycerol surfaces coated with PMMA particles are prepared as follows. First, the glycerol droplets and capillary bridges are prepared in contact with air in a capillary channel. Then, the channel is filled with particles suspended in the oil. Particles in the bulk can be removed by subsequently flushing the channel with clean oil. The PMMA particles, prepared following refs 26, 27, are coated with a layer of poly(hydroxy stearic acid) (PHSA), which charges positively ($\sim$100 charges per particle) in the oil[28]. The oil phase is a mixture of cyclohexyl bromide (CHB) and dodecane that matches the refractive index of glycerol, allowing us to image with minimal distortion the full surface even when it is highly curved (Fig. 1). The particles are highly hydrophobic, but nonetheless bind to the glycerol–oil interface by image charge attraction to the higher dielectric glycerol ($\varepsilon_{\mathrm{glycerol}}\approx 42$, $\varepsilon_{\mathrm{CHB}}\approx 7.9$)[28]. The dielectric contrast also drives the migration of ions from the oil phase into the glycerol, cleaning the oil above the interface, leading to a Debye screening length of $\sim$50 μm. Furthermore, positive ions are pumped from the oil to the water phase preferentially over negative ions, causing the glycerol to charge positively and repel residual particles suspended in the oil. These effects combine to create a clean lattice of strongly repulsive particles uninfluenced by particles in the bulk.

Imaging and reconstruction. Particles were imaged using a Yokogawa CSU-10 spinning disk confocal microscope and a Leica SP5 confocal microscope. Confocal images were rendered using Andor IQ. Particles were tracked using standard IDL tracking routines[29]. Triangulations and rendering were done using custom codes written in Matlab.

Received 29 July; accepted 25 October 2010.

1. Fuller, R. Building construction. US Patent US2682235, 1–12 (1954).
2. Bausch, A. R. *et al.* Grain boundary scars and spherical crystallography. *Science* **299,** 1716–1718 (2003).
3. Lipowsky, P., Bowick, M., Meinke, J., Nelson, D. & Bausch, A. Direct visualization of dislocation dynamics in grain boundary scars. Preprint at ⟨http://arxiv.org/abs/cond-mat/0506366⟩ (2005).
4. Einert, T., Lipowsky, P., Schilling, J., Bowick, M. & Bausch, A. Grain boundary scars on spherical crystals. *Langmuir* **21,** 12076–12079 (2005).
5. Nelson, D. & Peliti, L. Fluctuations in membranes with crystalline and hexatic order. *J. Phys.* **48,** 1085–1092 (1987).
6. Pérez-Garrido, A., Dodgson, M. & Moore, M. Influence of dislocations in Thomson's problem. *Phys. Rev. B* **56,** 3640–3643 (1997).
7. Bowick, M., Nelson, D. & Travesset, A. Interacting topological defects on frozen topographies. *Phys. Rev. B* **62,** 8738–8751 (2000).
8. Vitelli, V., Lucks, J. B. & Nelson, D. R. Crystallography on curved surfaces. *Proc. Natl Acad. Sci. USA* **103,** 12323–12328 (2006).
9. Santangelo, C., Vitelli, V., Kamien, R. & Nelson, D. Geometric theory of columnar phases on curved substrates. *Phys. Rev. Lett.* **99,** 017801 (2007).
10. Giomi, L. & Bowick, M. Defective ground states of toroidal crystals. *Phys. Rev. E* **78,** 010601 (2008).
11. Sausset, F., Tarjus, G. & Nelson, D. R. Structure and dynamics of topological defects in a glassy liquid on a negatively curved manifold. *Phys. Rev. E* **81,** 031504 (2010).
12. Hexemer, A. *Order and Disorder of Block Copolymers and Particles on Surfaces with Topology.* PhD thesis, Univ. California Santa Barbara (2006).
13. DeVries, G. A. *et al.* Divalent metal nanoparticles. *Science* **315,** 358–361 (2007).
14. Chaikin, P. & Lubensky, T. *Principles of Condensed Matter Physics* (Cambridge Univ. Press, 1995).
15. Nelson, D. *Defects and Geometry in Condensed Matter Physics* (Cambridge Univ. Press, 2002).
16. Lipowsky, P., Bowick, M., Meinke, J., Nelson, D. & Bausch, A. Direct visualization of dislocation dynamics in grain-boundary scars. *Nature Mater.* **4,** 407–411 (2005).
17. Bowick, M. J., Giomi, L., Shin, H. & Thomas, C. K. Bubble-raft model for a paraboloidal crystal. *Phys. Rev. E* **77,** 021602 (2008).
18. Hexemer, A., Vitelli, V., Kramer, E. & Fredrickson, G. Monte Carlo study of crystalline order and defects on weakly curved surfaces. *Phys. Rev. E* **76,** 051604 (2007).
19. Bowick, M. J. & Giomi, L. Two-dimensional matter: order, curvature and defects. *Adv. Phys.* **58,** 449–563 (2009).
20. Turner, A. M., Vitelli, V. & Nelson, D. R. Vortices on curved surfaces. *Rev. Mod. Phys.* **82,** 1301–1348 (2010).
21. Kamien, R. The geometry of soft materials: a primer. *Rev. Mod. Phys.* **74,** 953–971 (2002).
22. Gillette, R. & Dyson, D. Stability of fluid interfaces of revolution between equal solid circular plates. *Chem. Eng. J.* **2,** 44–54 (1971).
23. Langbein, D. W. *Capillary Surfaces: Shape-Stability-Dynamics, in Particular Under Weightlessness* (Springer, 2002).
24. Weertman, J. & Weertman, J. R. *Elementary Dislocation Theory* (Oxford Univ. Press, 1992).
25. Modes, C. D. & Kamien, R. D. Hard disks on the hyperbolic plane. *Phys. Rev. Lett.* **99,** 235701 (2007).
26. Bosma, G. *et al.* Preparation of monodisperse, fluorescent PMMA-latex colloids by dispersion polymerization. *J. Colloid Interface Sci.* **245,** 292–300 (2002).
27. Antl, L. *et al.* The preparation of poly(methyl methacrylate) lattices in nonaqueous media. *Colloids Surf.* **17,** 67–78 (1986).
28. Leunissen, M. E., van Blaaderen, A., Hollingsworth, A. D., Sullivan, M. T. & Chaikin, P. M. Electrostatics at the oil-water interface, stability, and order in emulsions and colloids. *Proc. Natl Acad. Sci. USA* **104,** 2585–2590 (2007).
29. Crocker, J. & Grier, D. Methods of digital video microscopy for colloidal studies. *J. Colloid Interface Sci.* **179,** 298–310 (1996).

Supplementary Information is linked to the online version of the paper at www.nature.com/nature.

Acknowledgements We acknowledge discussions with M. Bowick, A. Grosberg, S. Sacanna and A. M. Turner. W.T.M.I. acknowledges guidance in particle synthesis from A. D. Hollingsworth and M. T. Elsesser. W.T.M.I. acknowledges support from Rhodia and the English Speaking Union. P.M.C. acknowledges support from MRSEC DMR-0820341 and NASA NNX08AK04G. W.T.M.I. and V.V. acknowledge hospitality from Stichting FOM and the Aspen Center for Physics.

Author Contributions P.M.C. and W.T.M.I. initiated and designed research. W.T.M.I. designed and performed experiments, analysed data and synthesized colloidal particles. W.T.M.I., P.M.C and V.V. interpreted data. V.V. and W.T.M.I. performed elasticity calculations. W.T.M.I. and P.M.C. wrote the manuscript.

Author Information Reprints and permissions information is available at www.nature.com/reprints. The authors declare no competing financial interests. Readers are welcome to comment on the online version of this article at www.nature.com/nature. Correspondence and requests for materials should be addressed to W.T.M.I. (wtmirvine@uchicago.edu) and P.M.C. (chaikin@nyu.edu).